

# Multimaterial 3D Laser Printing of Cell-Adhesive and Cell-Repellent Hydrogels

*Niklas Schwegler, Tanisha Gebert, Maria Villiou, Federico Colombo, Barbara Schamberger, Christine Selhuber-Unkel\*, Franziska Thomas\*, and Eva Blasco\**

N. Schwegler, T. Gebert, Dr. M. Villiou, Dr. F. Colombo, Dr. B. Schamberger, Prof. Dr. C. Selhuber-Unkel, Prof. Dr. E. Blasco  
Institute for Molecular Systems Engineering and Advanced Materials  
Heidelberg University  
Im Neuenheimer Feld 225, 69120 Heidelberg  
E-Mail: [eva.blasco@oci.uni-heidelberg.de](mailto:eva.blasco@oci.uni-heidelberg.de), [selhuber@uni-heidelberg.de](mailto:selhuber@uni-heidelberg.de)

N. Schwegler, Jun.-Prof. Dr. F. Thomas, Prof. Dr. E. Blasco  
Institute of Organic Chemistry  
Heidelberg University  
Im Neuenheimer Feld 270, 69120 Heidelberg  
E-Mail: [franziska.thomas@oci.uni-heidelberg.de](mailto:franziska.thomas@oci.uni-heidelberg.de)

**Keywords:** Cell adhesion, RGD, hydrogels, direct laser writing, two-photon

This study introduces a straightforward method for manufacturing 3D microstructured cell-adhesive and cell-repellent multimaterials using two-photon laser printing. Compared to existing strategies, this approach offers bottom-up molecular control, high customizability and rapid and precise 3D fabrication. The printable cell-adhesive PEG-based material includes an RGD-containing peptide synthesized through solid-phase peptide synthesis, allowing for precise control of the peptide design. Remarkably, minimal amounts of RGD peptide (< 0.1 wt%) suffice for imparting cell-adhesiveness, while maintaining identical mechanical properties in the 3D printed microstructures to those of the cell-repellent, PEG-based material. Fluorescent labeling of the RGD peptide facilitates visualization of its presence in cell-adhesive areas. To demonstrate the broad applicability of our system, we showcase the fabrication of cell-adhesive 2.5D and 3D structures, fostering the adhesion of fibroblast cells within these architectures. Thus, this approach allows for the printing of high-resolution, true 3D structures suitable for diverse applications, including cellular studies in complex environments.

# 1 Introduction

The extracellular matrix (ECM) represents the three-dimensional (3D) scaffold of cells in native tissue. Through mechanical, structural and biochemical cues, it regulates cellular processes such as adhesion, migration, differentiation, and apoptosis.<sup>[1]</sup> While cells are still predominantly cultured in two-dimensional environments, the improved understanding of the influence of the third dimension on cellular processes has led to a shift towards ECM-mimetic 3D materials for cell culturing, such as scaffolds<sup>[2]</sup>, spheroids<sup>[3]</sup> and capsules<sup>[4]</sup>. This opens the possibility of preserving or manipulating natural cell behavior. Starting from early studies on the influence of material stiffness on stem cell differentiation, “3D cell culture” has emerged as a highly innovative field of research.<sup>[5]</sup> Biomedical applications in regenerative medicine and tissue engineering as well as fundamental studies of cell behavior have been considerably advanced through the development of synthetic ECM-like materials.<sup>[6]</sup> 3D printing or additive manufacturing techniques are among the most popular fabrication methods for 3D environments for cell culturing.<sup>[7]</sup> To allow manufacturing of complex structures at single-cell resolution, precise printing techniques are increasingly essential tools. Two-photon laser printing (2PLP), also known as two-photon direct laser writing, allows for fabrication of complex functional structures with submicron resolution features.<sup>[8]</sup> In 2PLP, a near-infrared femtosecond laser is focused into a liquid containing both photopolymerizable precursors and a photoinitiator. This photoresist or ink can be locally polymerized upon two-photon absorption within the focus point of the laser.<sup>[9]</sup>

Soft and biocompatible materials are suited as 3D scaffolds for cell culture with hydrogels being the most commonly used type of material in this context. There has been a recent surge in the development of hydrogel-producing inks for 2PLP.<sup>[10]</sup> Monomers and crosslinkers such as polyethylene glycol diacrylate (PEGDA) or acrylamide (AAm) are widely used for these purposes.<sup>[11]</sup> They are reliably printable and can be chemically synthesized in high purity, ensuring reproducible mechanical properties.<sup>[11-12]</sup> However, the final printed material must display cell-adhesive properties to allow cells to be cultured in or on it. Synthetic precursors like PEGDA or AAm are generally cell-repellent. Therefore, various strategies have been developed to impart cell-adhesiveness. Most commonly, pre-cured hydrogels are post-functionalized with cell-adhesive peptide motifs such as Arg-Gly-Asp (RGD).<sup>[13]</sup> Modification processes of this kind allow for high-resolution patterning and implementation of multiorthogonal cues, and the degree of cell adhesion and specificity to proteins can be tuned with high precision.<sup>[14]</sup> However, these approaches are usually multi-step processes that require careful optimization on a case-by-case basis. Besides post-functionalizing non-bioresponsive materials, 2PLP of acrylated and methacrylated natural polymers with cell-adhesive cues such as gelatine is often used.<sup>[10c, 15]</sup> These are readily available but, due to their natural origin, are limited by batch-to-batch variation and impurities that can affect the reproducibility of mechanical and functional properties.<sup>[16]</sup> In addition, non-specific chemical (meth)acrylation increases batch heterogeneity for these materials. Other concepts using natural cell-adhesive polymers involve pre- or post-modification steps and include, for example, coating of printed structures with fibronectin, an RGD-containing ECM protein or other cell-adhesive proteins.<sup>[2b, 17]</sup> An interesting approach that involves a PEG-protein hybrid material has been described by Song et al..<sup>[18]</sup> A PEGDA-based ink was combined with acrylated, RGD-containing recombinant proteins, allowing for the fabrication of multimaterials with cell-adhesive and cell-repellent patches. However, complete molecular control of material production was not given, as the recombinant protein ink was functionalized with methacrylate after recombinant synthesis, a multi-step process that is not site-selective and thus leads to mixtures of protein inks with different positioning and amounts of polymerizable groups.

All of the above methods of producing cell-adhesive materials face various challenges and limitations, due to the lack of complete and precise molecular control of the employed materials. Herein, we propose a straightforward approach to produce multimaterial 3D microstructures for cell culturing via 2PLP. Compared to previously reported strategies, our method enables easy and rapid material fabrication, bottom-up molecular control of the functional precursors, and a high degree of customizability. Our printable cell-adhesive PEG-based material includes an RGD-containing peptide chemically synthesized using solid-phase peptide synthesis (SPPS), thus allowing precise control of peptide-ink design (**Figure 1A**). Importantly, only small amounts of RGD peptide (1 mM, < 0.1 wt%) are required to achieve cell-adhesiveness in the PEG material. Therefore, structures printed with and without RGD show identical mechanical properties. We have utilized this advantage of our method to produce multimaterial structures with homogenous stiffness and cell-adhesive and cell-repellent patches. By fluorescently labelling the RGD peptide, we were able to visualize its presence in the cell-adhesive areas of these prints. To demonstrate the broad applicability of our material fabrication method in the field of 3D cell culture, we used our inks to print cell-adhesive 2.5D and 3D structures and cultured fibroblast cells within these architectures. Our method thus enables the printing of high-resolution, true 3D structures that can be used, e.g. for cell adhesion or migration studies in complex environments.

## 2 Results and Discussion

### 2.1 Ink Design and Method Development

Reliable and reproducible cell studies require cell-adhesive hydrogels that can be produced predictably and reproducibly with regard to their properties and functions. To this aim, we have chosen PEGDA (MW 575) as crosslinker and basic component for our material design. PEGDA has been widely used for the fabrication of very defined 3D hydrogel microstructures using 2PLP. However, this material is cell repellent.<sup>[11]</sup> To obtain cell adhesiveness we opted for a polymerizable peptide component with the adhesion motif RGD. An acrylate moiety was incorporated at the *N*-terminus for printability purposes, allowing rapid, local polymerization upon radical initiation, and ensuring a consistent polymerization mechanism during printing by using the same printable unit as for the crosslinker component.<sup>[19]</sup> Joined to the acrylate by a short PEG-linker, the fibronectin-derived cell-adhesive amino acid motif Gly-Arg-Gly-Asp-Ser (GRGDS) was implemented. Followed by a short glycine linker (...-Gly-Gly-...), a lysine (Lys, K) residue was introduced to balance the overall charge and ensure complete dissolution in the ink, thus circumventing problems of printability and reproducibility associated with a suspension ink. The peptide was chemically synthesized using solid-phase peptide synthesis (SPPS). The design and the chosen synthetic approach for the peptide ink is highly modular and allows a) an easy adjustment of the peptide sequence if a different motif is desired, b) the introduction of additional functional units such as fluorescent or affinity markers, e.g. 5(6)-carboxyfluorescein, and c) an easy adjustment of the distance of the adhesion motif to the material via the length of the PEG linker (**Figure 1B**).

The next step was to optimize the formulation and printing parameters of the reference PEG-based material. The formulation consisted of PEGDA as a crosslinker, and lithium phenyl (2,4,6-trimethylbenzoyl) phosphinate (LAP) as photoinitiator in aqueous solution. We found an optimum of printability with minimal use of LAP and PEGDA and with good and fast preparation of a homogenous solution with 50 wt% PEGDA and 2 wt% LAP in pure water. Tests with pH-buffered aqueous solutions in the ink led to LAP solubility limitations. The printed structures were developed in pure water overnight to wash out excess LAP and PEGDA. Delamination of printed structures from the glass substrate

was observed for large features (> 100  $\mu\text{m}$  lateral size) during subsequent treatment with isopropanol or ethanol, a necessary sterilization step in preparation for the cell experiments. Therefore, a surface functionalization procedure for the glass substrates was optimized. The final procedure involves extensive plasma treatment of the substrates followed by surface functionalization with an acrylated silyl ether. For structures printed on substrates functionalized with this procedure, no delamination effects were observed.

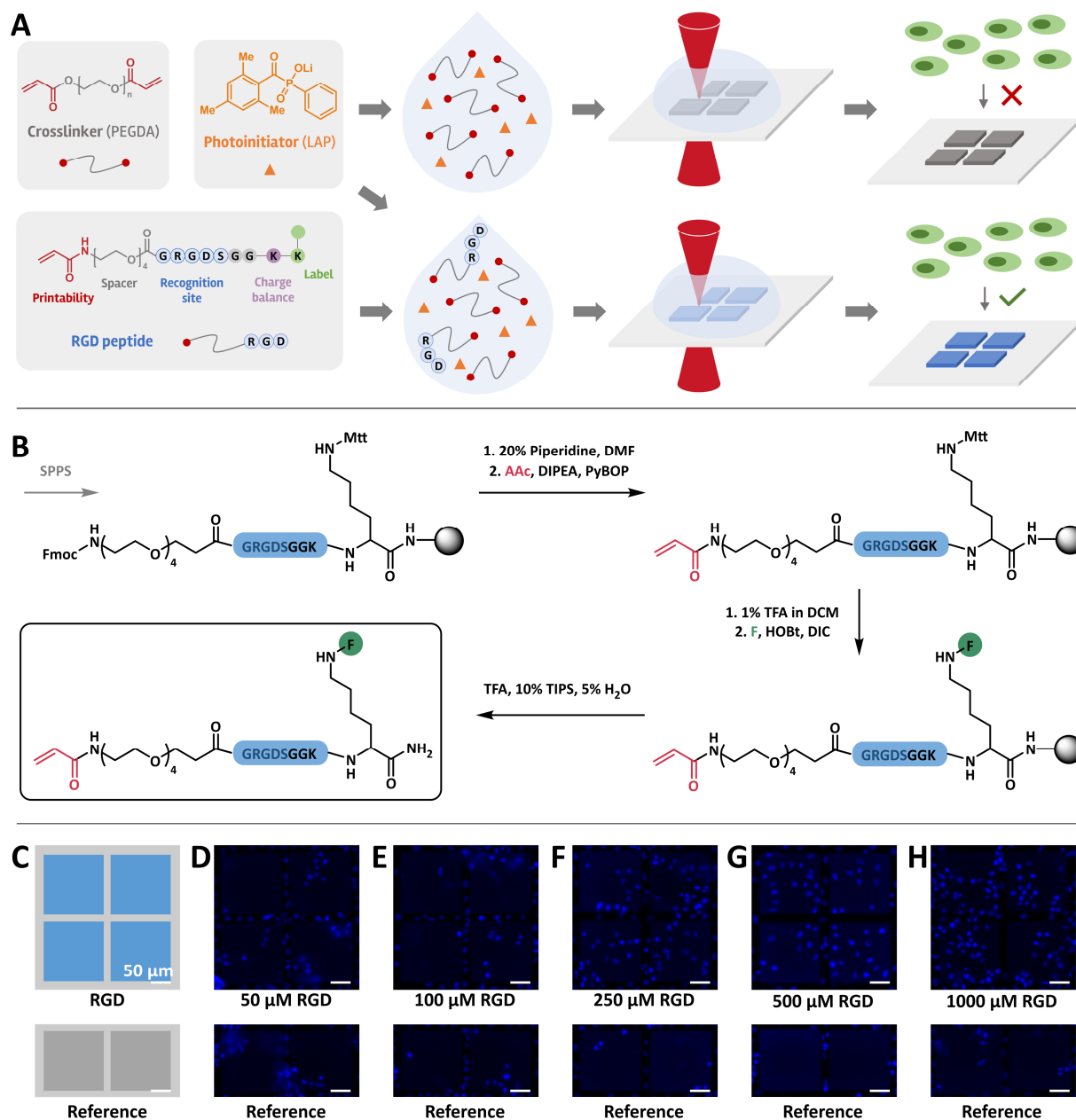


**Figure 1: Development of multimaterial 3D printing of cell-adhesive and cell-repellent hydrogels. (A)** Schematic representation of the ink design and the hydrogel manufacturing process. The ink assembly is followed by 2PLP. Depending on the ink applied, the printed structures can be used as cell-adhesive or cell-repellent 3D microenvironments for cell culturing. **(B)** Synthetic approach towards labelled RGD peptides. Fluorescence label ("F") was introduced via an orthogonal protecting group strategy. **(C)-(H)** Fluorescence images of stained cell nuclei showing cell adhesion on hydrogel blocks (150x150x12  $\mu\text{m}$ ) printed with inks with different RGD-peptide concentrations (Adhesion assay: Mammalian rat embryonic fibroblasts, incubation at 37  $^{\circ}\text{C}$  for 2 h): (C) Schematic representation of printed structures, (D) 50  $\mu\text{M}$ , (E) 100  $\mu\text{M}$ , (F) 250  $\mu\text{M}$ , (G) 500  $\mu\text{M}$ , (H) 1000  $\mu\text{M}$  RGD peptide. Corresponding control blocks (150x150x12  $\mu\text{m}$ , "reference") printed with reference ink (50 wt% PEGDA, 2 wt% LAP in water) are represented below each RGD block.

With the PEGDA ink formulation in hand, we investigated the printability of the RGD-peptide-PEGDA ink and the dependence of cell adhesion on the concentration of the RGD-peptide in the ink. For this purpose, the optimized printing parameters from the previously developed RGD-free, cell-repellent ink (“reference”) were used for the RGD-containing inks. All inks showed identical, excellent printability at these parameters. We printed five samples of different RGD-peptide concentrations, each with four 150x150x12  $\mu\text{m}$  blocks, and two blocks of reference ink of the same dimensions for each sample (**Figure 1C**). The reference material was not expected to show cell adhesion, as it does not contain any respective cues. It was therefore used as cell-repellent control for the cell adhesion assays. To test the cell adhesiveness of the materials, wild-type mammalian rat embryonic fibroblasts were seeded onto the samples. Fluorescence staining of the cell nuclei was performed for detailed visualization. The location of the cells on the printed blocks was then analyzed by fluorescence microscopy. Hydrogel blocks printed with 50  $\mu\text{M}$  and 100  $\mu\text{M}$  RGD-peptide concentration did not show significantly improved cell-adhesion properties compared to the reference structures (cell-adhesion selectivity ratio: 0.9 and 0.8 *RGD:Reference*, **Figure 1D-E**). When an RGD ink with a concentration of 250  $\mu\text{M}$  was used, significantly improved cell adhesion was observed compared to the reference with a selectivity ratio of 5.4 *RGD:Reference* and a total number of 65 cells on the four RGD blocks (**Figure 1F**). The sample printed with 500  $\mu\text{M}$  RGD-ink concentration displayed 56 adhered cells on its RGD blocks, while no cells were found on the reference blocks (**Figure 1G**). 1000  $\mu\text{M}$  RGD ink concentration yielded highly cell-adherent material samples, with 94 cells adhering to the RGD blocks (**Figure 1H**). However, the cell adhesion selectivity ratio of 5.2 *RGD:Reference* was similar to that obtained for the 250  $\mu\text{M}$  RGD sample. In summary, these results indicate a turning point in cell adhesiveness of the final material between 100  $\mu\text{M}$  and 250  $\mu\text{M}$  RGD ink concentration. This is in agreement with previous studies, where cell adhesion did not improve above a certain critical local RGD density on a 2D substrate.<sup>[20]</sup> To ensure good cell adhesion in further experiments, a concentration of 1000  $\mu\text{M}$  RGD peptide was chosen for the formulation of the cell-adhesive ink.

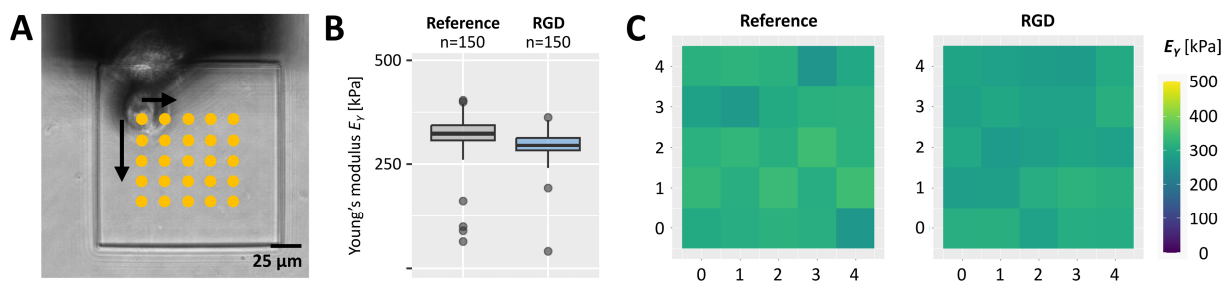


**Figure 2: Comparative mechanical analysis of printed blocks from cell-adhesive and cell-repellent ink. (A)** Schematic visualization of the matrix scan method employed for mechanical characterization. 5x5 indentations (20  $\mu\text{m}$  spacing) were performed for each hydrogel block. **(B)** Box plot of the Young's modulus of six different reference and six different RGD blocks ( $E_Y(\text{Ref}) = 322.6 \text{ kPa}$ ,  $E_Y(\text{RGD}) = 296.2 \text{ kPa}$ ). **(C)** Stiffness map of Young's modulus measurements for a single reference block (left) and for a single RGD block (right).

To test the mechanical stiffness of the printed materials, indentation studies were performed in Dulbecco's Modified Eagle Medium (DMEM) buffer. A set of six 150x150x12  $\mu\text{m}$  blocks each, printed with reference and RGD ink using the same parameters, was analyzed with 25 data points per block (**Figure 2A**). Identical mechanical properties were observed with an average Young's modulus of 322.6 kPa for reference blocks and 296.2 kPa for RGD blocks (**Figure 2B**). Despite statistical significance ( $p < 0.05$ ), the difference of 26.4 kPa is negligible when considering a standard deviation of 46.6 kPa for reference blocks and 33.8 kPa for RGD blocks. In addition, the samples showed excellent stiffness homogeneity within one block (**Figure 2C**) and across different blocks (**Figure 2B**). The inks therefore offer the possibility to print cell-repellent and cell-adhesive structures with similar mechanical

properties and chemical compositions, e.g. to produce patterned structures for guided cell adhesion. This is a clear advantage of our method, as similar mechanical and chemical properties within a multimaterial are highly important to avoid activation of mechanosensory pathways in the cells and a bias in the cellular signaling cascade.<sup>[18, 21]</sup>

## 2.2 Materials for Customized Cell Studies

Following the development and optimization of the basic manufacturing process, we aimed to demonstrate its versatility, particularly for customized applications in the field of 3D cell culture. The identical mechanical stiffness of structures printed with the cell-adhesive RGD ink and the cell-repellent reference ink opens up the possibility of manufacturing multimaterials with cell-repellent and cell-adhesive patches for controlled cell adhesion in the micrometer scale. This was demonstrated by designing and printing a chess-board-type multimaterial model. The model consisted of a 4x4 array of 150x150x12  $\mu\text{m}$  blocks with alternating cell-adhesion properties (**Figure 3A**). After seeding of fibroblast cells, adhesion on the RGD-containing blocks of the chess-board structures was observed (**Figure 3A-E**). Fluorescence staining of the cell nuclei and actin filaments confirmed successful selective cell culturing in the RGD-containing areas (**Figure 3C-D**).

To visualize the peptide localization within such a multimaterial scaffold, we printed another chess board structured multimaterial with fluorescent RGD-peptide (135  $\mu\text{M}$ ) added to the RGD ink (**Figures 1B, 3F-J**). As with the first structure (**Figure 3A-E**), selective cell adhesion to the RGD-containing blocks was observed, resulting in a sample with patterned cell-culturing areas. In addition, the fluorescent peptide could be visualized (excitation at 488 nm, **Figure 3I**), demonstrating perfect correspondence between cell adhesion and peptide incorporation (**Figure 3H-J**).

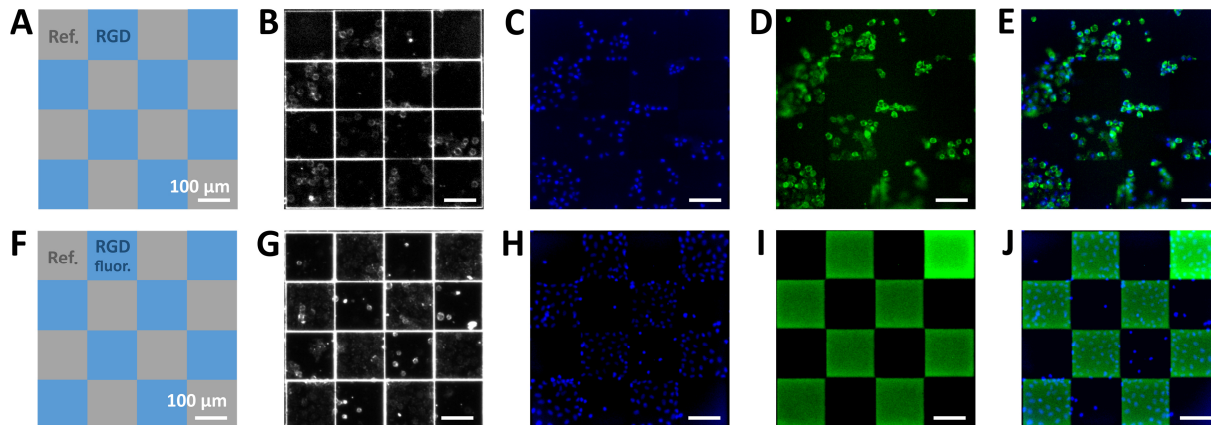


**Figure 3: Multimaterial prints for guided cell adhesion.** (Adhesion assay: Mammalian rat embryonic fibroblasts, incubation at 37 °C for 2 h). **(A)-(E)** Chess-board-like printed structures with alternating RGD and reference blocks (150x150x12  $\mu\text{m}$ ). **(A)** Schematic print model, **(B)** brightfield microscopy image, **(C)** fluorescence microscopy image showing stained cell nuclei, **(D)** fluorescence microscopy image showing stained actin filaments, **(E)** superimposed fluorescence microscopy images of cell nuclei and actin staining. **(F)-(J)** Chess-board-like printed structures with alternating RGD and reference blocks (150x150x12  $\mu\text{m}$ ). **(F)** Schematic print model, **(G)** brightfield microscopy image, **(H)** fluorescence microscopy image showing stained cell nuclei, **(I)** fluorescence microscopy image showing the (5,6)-carboxyfluorescein-labelled RGD peptide within the multimaterial ( $\lambda_{\text{ex}} = 488 \text{ nm}$ ), **(J)** superimposed fluorescence microscopy images of cell nuclei staining and fluorescently-labelled peptides in the multimaterial.

In addition to the ability to produce cell-adhesive materials with complete molecular control, 2PLP also opens up the possibility of printing 3D materials with micrometer-scale resolution. Taking advantage of this, we printed high-resolution 3D structures with our inks to investigate the spatial control over cell presence and adhesion. First, we printed 110x85x6  $\mu\text{m}$  lattices and preformed 15  $\mu\text{m}$  diameter wells in which to confine the cells, forcing the separation of individual cells. We used both the cell-

repellent reference ink and the cell-adhesive RGD ink and seeded both lattices with embryonic rat fibroblast cells (**Figures 4A-B, S6**). 3D reconstruction images obtained from confocal fluorescence microscopy showed that cells were trapped in only two wells of the reference lattice and did not spread across the wells separated by a lattice wall of 6  $\mu\text{m}$  height (**Figure 4A**). All other cells adhered exclusively to the underlying glass substrate without any connection in between trapped cells within the lattice. In contrast, significantly more cells colonized the wells of the RGD lattice. In addition, cytoskeletal overgrowth of large areas of the RGD lattice was observed, which could be visualized by staining of the cellular actin filaments (**Figure 4B**).

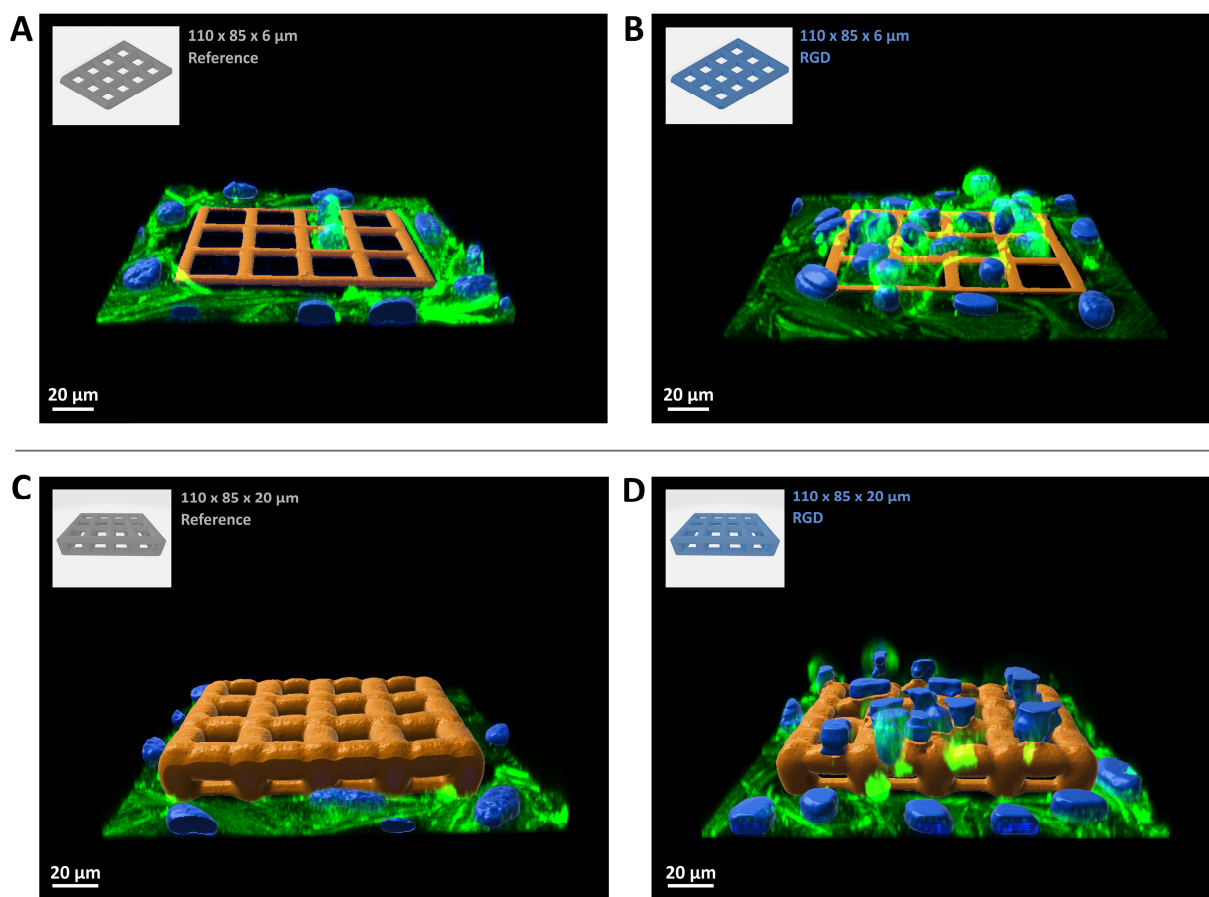


**Figure 4: 3D printed microstructured cell environments.** (Adhesion assay: Mammalian rat embryonic fibroblasts, incubation at 37 °C for 2 h). 3D structure models and 3D reconstruction images of the respective printed samples after cell seeding (Data obtained by 3D reconstructions from confocal microscopy; hydrogel in orange, cell nuclei in blue, actin filaments in green). **(A)-(B)** 2.5D lattices with 15  $\mu\text{m}$  wells. **(A)** Printed with reference ink, **(B)** printed with RGD ink. **(C)-(D)** 3D lattices with 15  $\mu\text{m}$  pores. **(C)** Printed with reference ink, **(D)** printed with RGD ink.

This example already shows the influence of both the cell-adhesive character of the material for 3D cell culture and the 3D structure. However, a lattice with a height of 6  $\mu\text{m}$  can be regarded as a mere 2.5D material that has limited influence on the spatial cell growth in a 3D cell culture. We therefore increased the environmental complexity and printed a “true” 3D lattice with dimensions 110x85x20  $\mu\text{m}$  and 15  $\mu\text{m}$  pores, again using cell-adhesive RGD ink and cell-repellent reference ink (**Figures 4C-D, S7**). The aim was to create porous, network-like environments to study cell adhesion and migration. Embryonic rat fibroblast cells were then seeded onto the reference and RGD lattice and cell nuclei and actin filaments were fluorescently stained. In 3D reconstructions obtained from confocal fluorescence microscopy images, the adhesion and growth of the cells along the lattice struts was observed on and within the RGD-containing lattices, with the cells pushing through the pores of the lattice (**Figure 4D**). In the lattices printed with reference ink, evasion of the cells towards the glass

support was observed (**Figure 4C**). It should also be noted that other, even more complex three-dimensional structures can be printed with the PEGDA and RGD-PEGDA inks. For example, a bent infinity sign was printed with RGD and reference ink (**Figure S8**). Cell adhesion was observed in all areas of these RGD-containing architectures with a network of intercellular cytoskeletal connections. Samples printed with RGD-free reference ink did not display cell adhesion.

### 3 Conclusion

A straightforward method for the preparation of multimaterial 3D hydrogels with cell-adhesive and cell-repellent areas, made exclusively from building blocks synthesized under complete molecular control, has been presented. The cell-adhesive material was prepared by 2PLP with an RGD-containing PEG-based ink thus ensuring even distribution of the adhesion motif throughout the printed material. An RGD peptide concentration of only 250  $\mu\text{M}$  is required to produce a material with excellent adhesion properties for fibroblast cells. In contrast, the materials printed with the peptide-free reference ink showed no cell adhesion. Mechanical analysis of cell-repellent and cell-adhesive printed blocks showed identical mechanical stiffness for both materials. The similar mechanical properties open up the possibility of printing multimaterials with cell-repellent and cell-adhesive areas and thus controlling cell adhesion. We demonstrated this using a chess board multimaterial model consisting of alternating cell-repellent and cell-adhesive patches. Fibroblast cells adhered exclusively to the RGD-containing areas. 2PLP also offers the possibility of printing 3D structures with micrometer resolution. Using 3D lattice structures, we have demonstrated that our RGD-functionalized ink can be used to print complex 3D structures for studying cell migration and guided cell adhesion. For instance, lattice-type architectures could be used to imitate porous cell environments or investigate confinement effects on cellular behavior.

Previously reported methods either involve multistep processes for the production of cell-adhesive materials or lack molecular control during the manufacturing of the building blocks for material production. The ink used in our 2PLP manufacturing approach was prepared from chemically synthesized precursor materials to ensure reproducible properties of both the inks and the final printed hydrogels. The design of the polymerizable peptide building block required to impart cell adhesiveness to the PEG-based material is highly modular, allowing easy customization of the peptide adhesion motif for a desired application and the introduction of additional functional moieties such as fluorescent or affinity markers. In fact, the RGD ink was used as a proof-of-concept for the development and optimization of the manufacturing process. We now envisage incorporating other adhesion motifs or different types of RGD peptides, e.g. with different affinities for integrins or even 3D-folded mini-proteins, into the inks, as such variations are of great importance for altering the stability of cell adhesion as well as for orthogonal functionalization strategies.<sup>[22]</sup> The modularity of our approach does not end with the peptide component for the cell-adhesive ink. Currently, our main material component is PEGDA, which is inexpensive and displays excellent gelling behavior during polymerization. However, we are confident that the simplicity of our manufacturing approach can be easily adapted to other photo crosslinking chemistries and thus to other crosslinking components.

In summary, the herein reported method provides potential users with a straightforward fabrication methodology for 3D-printed cell-adhesive hydrogels, while ensuring reproducible properties of both the ink as well as the final printed materials. Several customization options can be imagined due to the employed synthetic precursor materials, which display high molecular homogeneity and chemical modifiability. The method can be universally applied to produce microstructured 3D scaffolds for future cell studies in complex similar-to-native environments.

## 4 Experimental Section

**Solid-phase peptide synthesis:** RGD-peptides and labelled RGD peptides were synthesized with a CEM Liberty Blue microwave-assisted synthesizer. Syntheses were scaled to 0.1 mmol using Rink Amide MBHA PS resin as solid support. Stock solutions were prepared in DMF: 0.2 M Fmoc-protected amino acid solutions, 0.5 M DIC solution (activator), 1.0 M Oxyma<sup>®</sup> solution with 0.1 M DIPEA (activator base), and 20 vol% piperidine solution (deprotection). After synthesis, the resin was transferred to a 20 mL syringe with a PE frit. The resin was washed with 5x 5 mL DMF, 1x 5 mL dichloromethane, 1x 5 mL methanol, 1x 5 mL dichloromethane and dried *in vacuo* for further processing.

**RGD-peptide:** Acrylation was performed manually in a 20 mL syringe with a PE frit under yellow light conditions. Resin was combined with 35  $\mu$ L acrylic acid (0.5 mmol, 5.0 equivalents (eq.)), 260 mg PyBOP (0.5 mmol, 5.0 eq.), 175  $\mu$ L DIPEA (1.0 mmol, 10 eq.), and 5 mL DMF. The resin was equilibrated for 60 min, then washed with 5x 5 mL DMF and 2x 5 mL dichloromethane and dried *in vacuo*. Cleavage from the solid support was achieved by equilibrating the resin with a mixture of 8.5 mL TFA, 1.0 mL TIPS, and 0.5 mL water for 4 h. The solution was collected and the resin extracted with 2x 5 mL TFA. TFA was evaporated in a nitrogen stream from the combined extracts. At a finale volume of  $\sim$ 3 mL, 20 mL ice cold diethyl ether were added to precipitate the crude product. The peptide was isolated by centrifugation and decantation of the supernatant and washed with 2x 10 mL ice cold diethyl ether. The crude product was dissolved in 9 mL water and 1 mL MeCN (with 0.1% TFA). The peptide was lyophilized with a Christ Alpha 2-4-LDplus (equipped with a Vacuubrand RZ 6 pump) for further processing.

**Labelled RGD-peptide:** Acrylation as well as fluorescence labelling were performed manually in a 10 mL syringe with a PE frit under yellow light conditions. To allow for orthogonal labelling of the C-terminal lysine residue (K12), Fmoc-Lys(Mmt)-OH was used for the automated SPPS at this position. For the acrylation, 20  $\mu$ mol of resin were combined with 7  $\mu$ L acrylic acid (0.1 mmol, 5.0 eq.), 52 mg PyBOP (0.1 mmol, 5.0 eq.), 35  $\mu$ L DIPEA (0.2 mmol, 10 eq.), and 1.5 mL DMF. The resin was equilibrated for 60 min, then washed with 5x 3 mL DMF and 2x 3 mL dichloromethane and dried *in vacuo*. The Mmt-protecting group at the K12 position was removed by repeatedly adding 5 mL dichloromethane with 1.0 vol% TFA to the resin and equilibration for 60 seconds. Completion of the deprotection was indicated by the color of the deprotection solution after each iteration (yellow to colorless). The resin was then washed with 5x 5 mL dichloromethane. The peptide was fluorescently labelled using 94 mg 5(6)-carboxyfluorescein (250  $\mu$ mol, 12.5 eq.), 38 mg HOBt (250  $\mu$ mol, 12.5 eq.), 45  $\mu$ L DIC (15.0 eq.), and 1.5 mL DMF. The resin was equilibrated for 20 h, then washed with 5x 5 mL DMF and 2x 5 mL dichloromethane and dried *in vacuo*. Cleavage from the solid support was achieved by equilibrating the resin with a mixture of 4.25 mL TFA, 0.50 mL TIPS, and 0.25 mL water for 4 h. The peptide solution was collected and the resin extracted with 2x 2 mL TFA. TFA was evaporated in a nitrogen stream from the combined extracts. At a finale volume of  $\sim$ 1.5 mL, 10 mL ice cold diethyl ether were added to precipitate the crude product. The peptide was isolated by centrifugation and decantation of the supernatant and washed with 2x 5 mL ice cold diethyl ether. The crude product was dissolved in 4 mL water and 1 mL MeCN (with 0.1% TFA). The peptide was lyophilized with a Christ Alpha 2-4-LDplus (equipped with a Vacuubrand RZ 6 pump) for further processing.

**High-performance liquid chromatography:** High-performance liquid chromatography (HPLC) purification of the peptides was performed under yellow light conditions. The peptides were purified by reverse-phase HPLC on a Jasco system equipped with a PU-4180 pump, CO-4060 column thermostat, and UV-4070 detector. A Nucleodur<sup>®</sup> 100-5 C18ec (250x10 mm, 100  $\text{Å}$ , 5  $\mu$ m, MACHEREY-

NAGEL GmbH & Co. KG) column was used. A flow rate of 3 mL min<sup>-1</sup> and 50 °C oven temperature were applied. Analytical HPLC measurements were performed using a Hitachi system equipped with a 1110 Pump, 1210 auto sampler, 1310 column oven, and 1430 diode array detector. A VDSpher® PUR 100 C18-SE (250x4.6 mm, 100 Å, 5 µm, VDS optilab Chromatographietechnik GmbH) column was used. A flow rate of 1 mL min<sup>-1</sup> and 50 °C oven temperature were applied. Chromatograms at 220 nm were recorded during semipreparative and analytical HPLC. Water with 0.1% TFA (buffer A) and MeCN with 0.1% TFA (buffer B) were used as solvents. For the RGD peptide, method “5-30% B in A” was used, referring to 5 min initial equilibration at 5% B in A followed by a 30 min gradient from 5% B in A to 30% B in A (Figure S1). For the fluorescence labeled RGD peptide, method “15-35% B in A” was used, referring to 5 min initial equilibration at 15% B in A followed by a 30 min gradient from 15% B in A to 35% B in A (Figure S3).

*Mass spectrometry:* Matrix-assisted laser desorption ionization time-of-flight mass spectrometry (MALDI-TOF MS) was carried out on an Autoflex Speed device (Bruker Corporation). Samples were prepared by mixing 1 µL of sample solution with 1 µL of matrix solution (20 mg mL<sup>-1</sup> 2,5-dihydroxybenzoic acid in 30% MeCN and 0.1% TFA in water). The mixture was pipetted onto a steel target plate and left until dry. Used measuring mode is separately indicated for each spectrum (Figures S2, S4).

*Silanization procedure:* The procedure was performed under yellow light conditions. Glass substrates (22x22 mm, height 170±5 µm, Paul Marienfeld GmbH & Co.KG) were cleaned with isopropanol and acetone, then dried in a nitrogen stream. The glass surfaces were activated by treating them with a Harrick plasma cleaner (mode: high) for 45 min. Substrates were immersed in a 4 mM solution of 3-(trimethoxysilyl)propyl acrylate in toluene for 2.5 h. Substrates were washed with toluene (twice) and acetone, then dried in a nitrogen stream.

*Ink preparation:* The preparation was performed under yellow light conditions. LAP was dissolved in water and PEGDA (MW 575) to a final composition of 2.0 wt% LAP and 50.0 wt% PEGDA (reference ink). For RGD-peptide containing inks, respective volume of reference ink solution was added to aliquots of lyophilized pure peptide, yielding an ink solution of the desired RGD-peptide concentration.

*Two-photon laser printing:* 2PLP was performed using the Photonic Professional GT2 system (Nanoscribe GmbH). Structures were printed with a femtosecond laser (780 nm) focused with a 25x NA0.8 oil immersion objective (Carl Zeiss Microscopy GmbH). 3D models of STL format were processed with the Describe software package (Nanoscribe GmbH). Slicing and hatching were set to 0.3 µm with 90° hatching angle offset for each slice. Structures were printed at 50% laser power (with 100% calibrated to 50 mW) with a scan speed of 5 mm s<sup>-1</sup>. Inks were placed on a silanized glass substrate in a PDMS mold covered with a glass coverslip to prevent evaporation during printing. For multimaterial prints, the ink (RGD) was changed by immersing the prints in water for 5 min. The PDMS mold was then washed with the new ink (reference) by pipetting up and down 3x 10 times. The reference ink was applied a fourth time and the mold was covered with a fresh glass coverslip. If not stated otherwise, final printed structures were developed in water over night. Structures were stored in water until usage for cell adhesion assay.

*Cell adhesion assay:* Wild-type mammalian rat embryonic fibroblasts (REF-52wt) were cultured in DMEM supplemented with 10% fetal bovine serum (FBS) and 1% antibiotics (penicillin/streptomycin) at 37 °C in a humidified atmosphere containing 5% CO<sub>2</sub>. Cell culture medium was changed every second day. Cells from passage 10-20 were used. For seeding, print samples were placed in 6-well-plates. Wells were sterilized with 70% ethanol in water, washed two times with phosphate-buffered saline (PBS),

and once with DMEM. Next, 300 000 cells per well were seeded. Cells were incubated at 37 °C for 2 h, then fixed with 4% paraformaldehyde in PBS over night at 4 °C. For staining, cells were washed with PBS three times (5 min per wash). Next, they were incubated with Triton™ X-100 in Dulbecco's phosphate-buffered saline (DPBS) for 10 min, then washed with DPBS three times (5 min per wash). Blocking solution with 0.1% DPBS-Tween, 10% FBS and 3% bovine serum albumin (BSA) was added and samples were incubated at room temperature for 1 h. After blocking, cells were washed with 0.1% DPBS-Tween three times (5 min per wash). For the actin staining, rhodamine-phalloidin conjugate was applied in a 1:1000 dilution in blocking solution. After incubation at room temperature for 1 h on a shaker, samples were washed with 0.1% PBS-Tween three times (5 min per wash). For the nuclei staining, Hoechst-33342 was applied in a 1:1500 dilution in 0.1% PBS-Tween. After incubation at room temperature for 20 min, samples were washed with PBS. Fluorescence microscopy was performed with an Olympus IX81 device. Actin filaments were visualized by rhodamine-phalloidin excitation at 561 nm (emission detection at 575 nm), nuclei were visualized by Hoechst-33342 excitation at 360 nm (emission detection at 460 nm). 3D images were taken with a Nikon Ti2 Ax confocal light scanning microscope (Nikon Imaging Center, Heidelberg). Hoechst-33342 and hydrogel excitation were at 405 nm (emission detection at 430-475 nm). Rhodamine-phalloidin was excited at 561 nm (emission detection at 571-625 nm). The images were acquired using a Plan Apo  $\lambda$  S 25x C Sil objective. Images were segmented using Imaris (v 10.1.0).

*Mechanical characterization:* Indentation measurements were carried out using a Pavone Optics<sup>11</sup> Life device according to a previously published method.<sup>[23]</sup> A one-piece optical probe consisting of an optical fiber, a cantilever, and a spherical tip was approached onto printed hydrogel blocks in DMEM buffer. Cantilever deflection upon surface contact was detected with an interferometer, allowing for precise displacement measurements. A medium soft probe ( $k = 3.660 \text{ Nm}^{-1}$ ) with a spherical tip of 25  $\mu\text{m}$  diameter was used. Matrix scan measurements (5x5 data points per hydrogel block with 25  $\mu\text{m}$  xy distance between single points) were performed at a constant load of 1  $\mu\text{N}$  and a speed of 10  $\mu\text{m s}^{-1}$ . The collected data were analyzed with DataViewer V2.5.0. Force-indentation curves were fitted using the Hertz contact model with a constant indentation depth of 200  $\mu\text{m}$  ( $P_{\text{max}}\%$  for contact point = 50, Poisson's ratio = 0.5), yielding elastic moduli as well as  $R^2$  values of the fits. Resultant data were analyzed with R studio, and finally visualized after filtering the curves (for  $R^2 > 0.9$ ).

## Acknowledgements

N.S. is grateful to the Evangelisches Studienwerk Villigst e.V. for support through a Doctoral Scholarship and to the Joachim Herz Foundation for support through the Add-On Fellowship for Interdisciplinary Life Sciences. This work has been funded by the Spotlight Project Synthetic Immunology of the Flagship Initiative Engineering Molecular Systems (FI EMS) at Heidelberg University, which is funded by the Federal Ministry of Education and Research (BMBF) and the Ministry of Science Baden-Württemberg within the framework of the Excellence Strategy of the Federal and State Governments of Germany. We are grateful for support from the Deutsche Forschungsgemeinschaft (DFG, German Research Foundation) under Germany's Excellence Strategy via the Excellence Cluster "3D Matter Made to Order" (3DMM2O, EXC-2082/1-390761711). C. S. U., M. V. and F. C. also thank the European Research Council (ERC) for support through the Consolidator Grant PHOTOMECH (Grant no. 101001797) and the Volkswagen Foundation through the Initiative "Life?," Az. 96733. This research was conducted within the Max Planck School Matter to Life supported by the German Federal Ministry of Education and Research (BMBF) in collaboration with the Max Planck Society. We thank the Nikon Imaging Center

and the “Soft (bio)materials characterization” Core Facility (IMSEAM) at Heidelberg University for their support. We thank Målin Schmidt for support with two-photon laser printing for ink development.

## References

- [1] a) A. D. Theocharis, S. S. Skandalis, C. Gialeli, N. K. Karamanos, *Adv. Drug Del. Rev.* **2016**, 97, 4; b) C. Frantz, K. M. Stewart, V. M. Weaver, *J. Cell Sci.* **2010**, 123, 4195; c) A. D. Theocharis, S. S. Skandalis, G. N. Tzanakakis, N. K. Karamanos, *FEBS J.* **2010**, 277, 3904; d) R. V. Iozzo, R. D. Sanderson, *J. Cell. Mol. Med.* **2011**, 15, 1013; e) A. D. Theocharis, C. Gialeli, P. Bouris, E. Giannopoulou, S. S. Skandalis, A. J. Aletras, R. V. Iozzo, N. K. Karamanos, *FEBS J.* **2014**, 281, 5023; f) S. Schmidt, P. Friedl, *Cell Tissue Res.* **2010**, 339, 83.
- [2] a) K. Siemsen, S. Rajput, F. Rasch, F. Taheri, R. Adlung, J. Lammerding, C. Selhuber-Unkel, *Adv. Healthc. Mater.* **2021**, 10, 2100625; b) B. Richter, V. Hahn, S. Bertels, T. K. Claus, M. Wegener, G. Delaittre, C. Barner-Kowollik, M. Bastmeyer, *Adv. Mater.* **2017**, 29, 1604342.
- [3] a) S. Lagies, M. Schlimpert, S. Neumann, A. Wäldin, B. Kammerer, C. Borner, L. Peintner, *Commun. Biol.* **2020**, 3; b) H. Cui, X. Wang, J. Wesslowski, T. Tronser, J. Rosenbauer, A. Schug, G. Davidson, A. A. Popova, P. A. Levkin, *Adv. Mater.* **2021**, 33, 2006434.
- [4] Ö. Ertekin, M. Monavari, R. Krüger, M. Fuentes-Chandía, B. Parma, G. Letort, P. Tripal, A. R. Boccaccini, A. K. Bosserhoff, P. Ceppi, M. Kappellmann-Fenzl, A. Leal-Egaña, *Acta Biomater.* **2022**, 142, 208.
- [5] a) F. Pampaloni, E. G. Reynaud, E. H. K. Stelzer, *Nat. Rev. Mol. Cell Biol.* **2007**, 8, 839; b) A. J. Engler, S. Sen, H. L. Sweeney, D. E. Discher, *Cell* **2006**, 126, 677; c) D. E. Discher, D. J. Mooney, P. W. Zandstra, *Science* **2009**, 324, 1673; d) D. E. Discher, P. Janmey, Y.-l. Wang, *Science* **2005**, 310, 1139.
- [6] a) B. V. Slaughter, S. S. Khurshid, O. Z. Fisher, A. Khademhosseini, N. A. Peppas, *Adv. Mater.* **2009**, 21, 3307; b) D. Huh, G. A. Hamilton, D. E. Ingber, *Trends Cell Biol.* **2011**, 21, 745; c) B. A. Justice, N. A. Badr, R. A. Felder, *Drug Discov. Today* **2009**, 14, 102.
- [7] M. J. Lerman, J. Lembong, G. Gillen, J. P. Fisher, *Appl. Phys. Rev.* **2018**, 5.
- [8] a) R. D. Murphy, C. Delaney, S. Kolagatla, L. Florea, C. J. Hawker, A. Heise, *Adv. Funct. Mater.* **2023**, 33; b) Y. Lin, J. Xu, *Adv. Opt. Mater.* **2018**, 6, 1701359; c) M. Deubel, G. Von Freymann, M. Wegener, S. Pereira, K. Busch, C. M. Soukoulis, *Nature Mater.* **2004**, 3, 444.
- [9] A. Selimis, V. Mironov, M. Farsari, *Microelectron. Eng.* **2015**, 132, 83.
- [10] a) P. Mainik, C. A. Spiegel, E. Blasco, *Adv. Mater.* **2023**, DOI: 10.1002/adma.202310100; b) J.-F. Xing, M.-L. Zheng, X.-M. Duan, *Chem. Soc. Rev.* **2015**, 44, 5031; c) S. You, J. Li, W. Zhu, C. Yu, D. Mei, S. Chen, *J. Mater. Chem. B* **2018**, 6, 2187.
- [11] J. Torgersen, X.-H. Qin, Z. Li, A. Ovsianikov, R. Liska, J. Stampfl, *Adv. Funct. Mater.* **2013**, 23, 4542.
- [12] J. L. Drury, D. J. Mooney, *Biomaterials* **2003**, 24, 4337.
- [13] a) M. Barczyk, S. Carracedo, D. Gullberg, *Cell Tissue Res.* **2010**, 339, 269; b) C. Barner-Kowollik, M. Bastmeyer, E. Blasco, G. Delaittre, P. Muller, B. Richter, M. Wegener, *Angew. Chem. Int. Ed.* **2017**, 56, 15828; c) C. Bednarek, U. Schepers, F. Thomas, S. Bräse, *Adv. Funct. Mater.* **2023**, 2303613; d) S. H. Lee, J. J. Moon, J. L. West, *Biomaterials* **2008**, 29, 2962; e) J. C. Hoffmann, J. L. West, *Soft Matter* **2010**, 6, 5056; f) J. C. Culver, J. C. Hoffmann, R. A. Poché, J. H. Slater, J. L. West, M. E. Dickinson, *Adv. Mater.* **2012**, 24, 2344; g) X. H. Qin, X. Wang, M. Rottmar, B. J. Nelson, K. Maniura-Weber, *Adv. Mater.* **2018**, 30, 1705564; h) C. A. DeForest, K. S. Anseth, *Nat. Chem.* **2011**, 3, 925; i) C. A. DeForest, K. S. Anseth, *Angew. Chem. Int. Ed.* **2012**, 51, 1816.
- [14] T. G. Kapp, F. Rechenmacher, S. Neubauer, O. V. Maltsev, E. A. Cavalcanti-Adam, R. Zarka, U. Reuning, J. Notni, H.-J. Wester, C. Mas-Moruno, J. Spatz, B. Geiger, H. Kessler, *Sci. Rep.* **2017**, 7, 39805.
- [15] a) M. Carlotti, V. Mattoli, *Small* **2019**, 15, 1902687; b) J. Song, C. Michas, C. S. Chen, A. E. White, M. W. Grinstaff, *Adv. Healthc. Mater.* **2020**, 9, 1901217; c) M. Taale, B. Schamberger, F. Taheri, Y. Antonelli, A. Leal-Egaña, C. Selhuber-Unkel, *Adv. Funct. Mater.* **2023**, 2302356; d) P. Bajaj,

- R. M. Schweller, A. Khademhosseini, J. L. West, R. Bashir, *Annu. Rev. Biomed. Eng.* **2014**, 16, 247.
- [16] A. Ahmady, N. H. Abu Samah, *Int. J. Pharm.* **2021**, 608, 121037.
- [17] a) A. Arslan, K. Vanmol, A. Dobos, A. Natale, J. Van Hoorick, P. Roose, H. Van Den Bergen, T. Chalyan, A. Ovsianikov, S. Baudis, V. Rogiers, T. Vanhaecke, R. M. Rodrigues, H. Thienpont, J. Van Erps, S. Van Vlierberghe, P. Dubruel, *Biomacromolecules* **2021**, 4919; b) A. Rengaraj, L. Bosc, P. Machillot, C. McGuckin, C. Milet, N. Forraz, P. Paliard, D. Barbier, C. Picart, *ACS Appl. Mater. Interfaces* **2022**, 14, 13107.
- [18] J. Song, C. Michas, C. S. Chen, A. E. White, M. W. Grinstaff, *Macromol. Biosci.* **2021**, 21, 2100051.
- [19] L. Schittecatte, V. Geertsen, D. Bonamy, T. Nguyen, P. Guenoun, *MRS Commun.* **2023**, 13, 357.
- [20] E. A. Cavalcanti-Adam, T. Volberg, A. Micoulet, H. Kessler, B. Geiger, J. P. Spatz, *Biophys. J.* **2007**, 92, 2964.
- [21] a) S. B. Gutekunst, C. Grabosch, A. Kovalev, S. N. Gorb, C. Selhuber-Unkel, *Beilstein J. Nanotechnol.* **2014**, 5, 1393; b) A. W. Holle, A. J. Engler, *Curr. Opin. Biotechnol.* **2011**, 22, 648; c) J. Christian, J. W. Blumberg, D. Probst, C. Lo Giudice, S. Sindt, C. Selhuber-Unkel, U. S. Schwarz, E. A. Cavalcanti-Adam, *J. Vis. Exp.* **2022**, DOI: 10.3791/63121.
- [22] D. Pallarola, I. Platzman, A. Bochen, E. A. Cavalcanti-Adam, M. Axmann, H. Kessler, B. Geiger, J. P. Spatz, *BioNanoMaterials* **2017**, 18.
- [23] F. Colombo, M. Villiou, F. Taheri, L. Fröhlich, M. Taale, V. Albert, Q. Jiang, C. Selhuber-Unkel, *Adv. NanoBiomed Res.* **2023**, 3.